npj | Quantum Information

www.nature.com/npjqi

ARTICLE OPEN

Check for updates

# Quantum Hall phases emerging from atom–photon interactions

Alexander V. Poshakinskiy[1], Janet Zhong[2], Yongguan Ke[2,3], Nikita A. Olekhno[4], Chaohong Lee[3,5], Yuri S. Kivshar[2,4]✉ and Alexander N. Poddubny[1,2,4]✉

We reveal the emergence of quantum Hall phases, topological edge states, spectral Landau levels, and Hofstadter butterfly spectra in the two-particle Hilbert space of an array of periodically spaced two-level atoms coupled to a waveguide (waveguide quantum electrodynamics). While the topological edge states of photons require fine-tuned spatial or temporal modulations of the parameters to generate synthetic magnetic fields and the quantum Hall effect, here we demonstrate that a synthetic magnetic field can be self-induced solely by atom–photon interactions. The fact that topological order can be self-induced in what is arguably the simplest possible quantum structure shows the richness of these waveguide quantum electrodynamics systems. We believe that our findings will advance several research disciplines including quantum optics, many-body physics, and nonlinear topological photonics, and that it will set an important reference point for the future experiments on qubit arrays and quantum simulators.

*npj Quantum Information* (2021)7:34 ; https://doi.org/10.1038/s41534-021-00372-8

## INTRODUCTION

Recent technological advances have underpinned the rapid development of cavity quantum electrodynamics (QED) and circuit QED, which allow to exploit quantum properties of light for applications in information processing[1–3]. A closely related subfield with growing theoretical and experimental interest is waveguide QED[4,5], which studies one-dimensional arrays of natural or artificial atoms coupled to a waveguide. Existing platforms for waveguide QED systems include cold atoms[6], defect centers[7], superconducting qubits[2,3,8–12], and emerging structures based on exciton-polaritons[13].

Waveguide QED is promising for many applications in quantum information processing. It can allow us to efficiently generate[14–16], detect[17], slow[18], and store quantum light[19]. It is also useful as a platform for quantum simulators of complex many-mode physics[20,21]. A crucial advantage of waveguide QED systems is that they can exhibit long-range coupling between distant atoms mediated by light. This makes the dispersion of atomic excitations and their interactions markedly different from those in the typical case of nearest-neighbor coupling in circuit QED[1] or in conventional condensed matter systems. Thus, previously uncharted physical regimes can be naturally accessed in these waveguide-based quantum simulators.

The goal of this work is to explore the potential of waveguide QED to simulate quantum many-body topological phases of interacting matter. Topological phases underpin many concepts of modern matter physics. Topological edge states of electrons are usually created using magnetic fields[22] or spin–orbit interactions[23–25]. Studies of the quantum Hall effect and topological insulators have also inspired rapid progress in *topological photonics* where the central goal is to create robust edge states of light immune to disorder[26–29]. Since the effects of magnetic fields on light are weak, the realization of topological concepts in photonics requires artificial structures or metamaterials[30]. Alternative approaches rely on time modulation of structure parameters[31–34] or engineered nonlinearities[35,36]. These techniques create effective gauge fields in real or synthetic dimensions, and mimic the effects of magnetic fields or spin–orbit couplings for photons.

Here, we uncover that the hallmarks of quantum Hall phases, Landau energy levels, topological edge states, and the Hofstadter butterfly spectrum[37–39] naturally arise in a finite one-dimensional array of closely spaced two-level atoms (qubits) coupled to photons in a waveguide, shown in Fig. 1a. The striking feature of our prediction is that the quantum Hall phase can emerge solely from interactions of indistinguishable particles without any external magnetic fields or special fine tuning or modulation of spatial or temporal parameters.

While the proposed idea requires highly coherent structures, it could potentially be tested in already available arrays of superconducting qubits coupled to waveguides[40] using the existing approaches to probe spatial profile of two-photon quantum states[41]. Our results open the way to engineer complex multi-photon states and realize their topological protection against disorder.

## RESULTS

### Interaction-induced topological states

Here, we show how to realize topological quantum Hall phases from atom–photon interactions. In waveguide QED setups (shown schematically in Fig. 1a), photons become strongly coupled to atoms and create light-matter quasi-particles called *polaritons*. These polaritons are not independent but are strongly interacting, because one atom cannot absorb two photons simultaneously[42], leading to on-site repulsion. While the considered model is paradigmatic for quantum optics[4,5,43], its two-particle Hilbert space was not analyzed until recently. As shown in Fig. 1c, d, when

[1]Ioffe Institute, St. Petersburg, Russia. [2]Nonlinear Physics Centre, Research School of Physics, Australian National University, Canberra, ACT, Australia. [3]Guangdong Provincial Key Laboratory of Quantum Metrology and Sensing & School of Physics and Astronomy, Sun Yat-Sen University (Zhuhai Campus), Zhuhai, China. [4]ITMO University, St. Petersburg, Russia. [5]State Key Laboratory of Optoelectronic Materials and Technologies, Sun Yat-Sen University (Guangzhou Campus), Guangzhou, China. ✉email: ysk@internode.on.net; poddubny@coherent.ioffe.ru

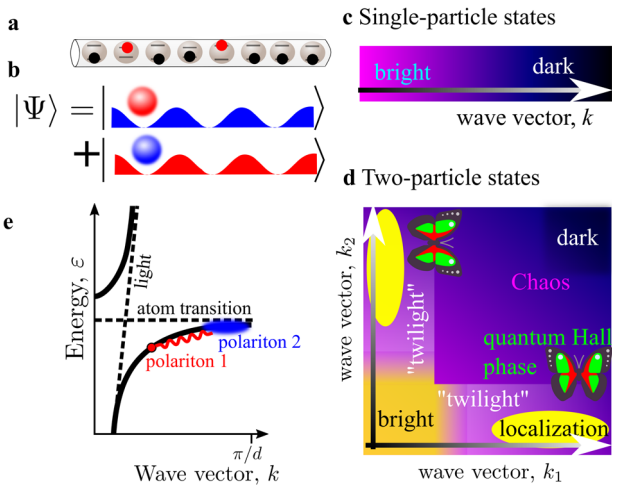


**Fig. 1 Emergence of two-polariton quantum phases from interactions. a** Double-excited one-dimensional array of two-level atoms (qubits) in a waveguide. **b** Two-polariton quantum states where each indistinguishable polariton induces a potential for the other one. **c** and **d** Classification of single- and double- excited states of the atomic array depending on the wave vector of the excitations. Butterflies in **d** indicate the regions where the quantum Hall phase and Hofstadter-like butterfly spectrum emerge from the interaction of two excitations. Regions of "twilight" states[47] and interaction-induced localization[48] are also shown. **e** Single-particle polariton dispersion. Interaction of a lower-branch polariton with small $k$ and that with large $k$ is illustrated.

the polariton wave vector is comparable with that of light, a collective atomic state is easily excited optically, and it generally gets "darker" for larger wave vectors. In a two-particle "bright" state, the wave vectors of both excitations are small, which corresponds to Dicke superradiance[44,45]. Two-particle dark states where both wave vectors are large were predicted only last year. These states originate from the fermionization of strongly interacting polaritons[46]. It has also been suggested that interactions in the corner regions[47] of the diagram of Fig. 1d can localize one of the two polaritons in the center of the array[48].

In this paper, we predict topological edge states driven by polariton–polariton interactions in the regions indicated by butterflies in Fig. 1d. In this region for a finite array, one polariton forms a standing wave with multiple nodes and a periodic potential for the other indistinguishable polariton, see Fig. 1b, e. As a result, the interaction is described by the *self-induced* Aubry-André-Harper[49] model that is mathematically equivalent to the quantum Hall problem on a lattice[50,51].

The periodic modulation is an intrinsic feature that arises naturally due to the polariton–polariton interactions, in sharp contrast to previous studies[52,53] where the modulation is imposed deliberately either by engineering the lattice[53,54] or applying external fields[29,33]. We show that the full Hofstadter butterfly-like spectrum could be obtained in a single shot from just a fixed atomic array, eliminating the need to continuously tune an external magnetic field in a conventional setup[33,39].

## Two-polariton states

The considered periodic one-dimensional array of $N$ two-level atoms (qubits) coupled to light is described by an effective Dicke-type Hamiltonian[46,47,55]

$$H = \sum_{n=1}^{N} \omega_0 \sigma_n^\dagger \sigma_n - i\Gamma_0 \sum_{n,m=1}^{N} e^{i\omega_0 d|n-m|/c} \sigma_n^\dagger \sigma_m, \quad (1)$$

where $c$ is the speed of light, $\sigma_n^\dagger$ is the operator creating excitation of the atom $n$ with the resonance frequency $\omega_0$, $(\sigma_n^\dagger)^2 = 0$ and $\Gamma_0$ is the radiative decay rate of a single atom. While for $d = 0$ the Hamiltonian (1) is equivalent to the conventional Dicke model[44], even small interatomic spacings $0 < d \ll 2\pi c/\omega_0$ make the model considerably richer.

Single-particle eigenstates of Eq. (1) in the infinite array ($N \to \infty$) are polaritons with the energy dispersion $\varepsilon(k) = \Gamma_0 \sin\varphi/(\cos k - \cos\varphi)$[55,56], which is shown schematically in Fig. 1e. The eigenstates are Bloch waves with real energies, characterized by continuous distribution of the wave vectors $-\pi/d < k < \pi/d$. The dispersion consists of two polaritonic branches, resulting from the avoided crossing of light with the atomic resonance where both branches are described by the same expression $\varepsilon(k)$. The upper branch corresponds to $|k| < \omega_0 d/c$ and in this work we focus on the lower branch with large wave vectors, $|k| > \omega_0 d/c$. In the finite array of $N$ atoms, the wave vectors are quantized, $k_j d = \pi j/N$, $j = 1, 2, \ldots N$[57], and the single-particle eigenstates are standing waves, as shown in Fig. 2a–d. Owing to the possibility of radiative decay into the waveguide, the eigenstates of the finite array (shown in Fig. 2a) have non-zero imaginary energies, $\mathrm{Im}\varepsilon < 0$[46]. Our main results below are obtained for strongly subradiant states where $|\mathrm{Im}\varepsilon| \ll \Gamma_0$. They are not qualitatively affected by the radiative losses and remain valid even when the non-Hermitian part of the Hamiltonian Eq. (1) is neglected (see Supplementary Fig. 5). Crucially, the spectrum in Fig. 2a condenses near the resonance $\varepsilon = \omega_0$, where the group velocity of polaritons decreases.

Next, we proceed to the double-excited states $\Psi = \sum_{n,m} \psi_{nm} \sigma_n^\dagger \sigma_m^\dagger |0\rangle$. Their spectrum, obtained from the Schrödinger equation $H\Psi = 2\varepsilon\Psi$, is shown in Fig. 2e–h in different energy scales. The spectrum consists of distinct groups of states with close energies. The distributions of the two-particle eigenvalue energies are plotted in the complex plane in Fig. 2e–g, and their shape resembles the sum of two single-particle eigenvalues (the single-particle spectra is plotted in Fig. 2a). This means that most states in Fig. 2e–g can be described by $\varepsilon \approx (\varepsilon_j + \varepsilon_i)/2$, where $\varepsilon_j$ and $\varepsilon_i$ are the single-particle energies from Fig. 2a. However, the dense part of the group, which corresponds to $\varepsilon_i \to \omega_0$ (see red arrows in Fig. 2f), is drastically transformed by the interaction. Three characteristic states from the group with $j = 7$ are presented in Fig. 2i–k. While the state in Fig. 2i is just a symmetrized product of two standing waves, weakly modified by interaction, the role of the interaction dramatically increases for $\mathrm{Re}\varepsilon - \omega_0 > -0.66\Gamma_0$ in Fig. 2h. The spectrum is split by interaction into relatively delocalized states with smaller radiative decay rate (yellow ellipse in Fig. 2h, k) and states with larger radiative losses where one of the two polaritons is localized at the edge of the structure (blue ellipse in Fig. 2h, j).

This interaction-induced transformation of the two-polariton spectrum is our central result. The delocalized states are almost $(j-1)$-fold degenerate, where $j$ is the group number and correspond to the Landau levels in the effective magnetic field. The states in Fig. 2j come in degenerate pairs corresponding to topological edge states localized at the opposite sides of the array.

## Landau levels, topological edge states, and Hofstadter butterfly

We now present an analytical model explaining the topological origin behind the interaction-induced edge states in Fig. 2j. In the basis $|x\rangle = \frac{1}{\sqrt{N}} \sum_{n=1}^{N} \exp(i\omega_0 d|x-n|/c) \sigma_n^\dagger |0\rangle$, $x = 1, 2, \ldots N$[48,58], the following ansatz can be used for the two-polariton state

$$\psi_{xy} = \psi_y^{(j)} \chi_x + \psi_x^{(j)} \chi_y, \quad x, y = 1 \ldots N \quad (2)$$

where $\psi_x^{(j)}$ and $\chi_x$ are the wavefunctions of the first and second polaritons. The former corresponds well to the standing wave $\psi_x^{(j)} = \cos k_j (x - \frac{1}{2})$. To determine the latter, we derive the Schrödinger equation that accounts for interaction between the

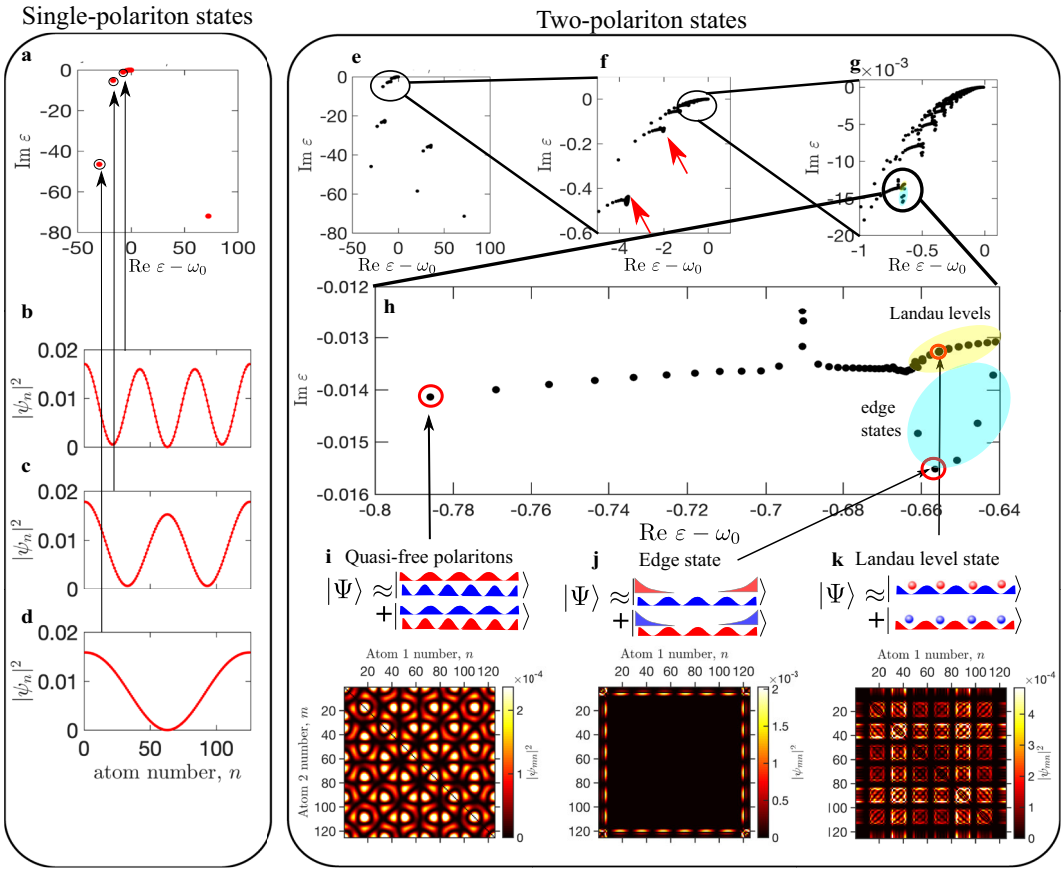


**Fig. 2 Single- and two-polariton energy spectra. a** complex energy spectrum of single-polariton modes. Three characteristic eigenstates are shown in panels **b**–**d**. **e**–**h** Two-polariton energy spectrum zoomed in different scales. **i**, **j**, **k** Spatial color maps of different characteristic two-polariton eigenstates $|\psi_{nm}|^2$. Calculation has been performed for $N = 125$ atoms and $\omega_0 d/c = 0.02$. Energy is measured in units of $\Gamma_0$.

polaritons. It is given by (see "Methods" for more details)

$$X_{x+1} + X_{x-1} - 2X_x + \left\{\frac{\omega_0+\omega_j-2\varepsilon}{2\varphi\Gamma_0} + \frac{4}{Nk_j^2}\cos^2\left[k_j\left(x-\frac{1}{2}\right)\right]\right\}^{-1} X_x = 0, \quad (3)$$

where $\omega_j \approx \omega_0 - 2\varphi\Gamma_0/k_j^2$ is the real part of the eigenfrequency of the single-polaritonic state $\psi^{(j)}$ and $\varphi = \omega_0 d/c$. Equation (3) describes a motion of a particle on a lattice in an external potential of a standing wave with the period $N/j$. It has a striking similarity to the Harper equation for an electron moving in a square lattice subjected to the perpendicular magnetic field[59]:

$$X_{x+1} + X_{x-1} + 2\cos(2\pi x\alpha - k_y)X_x = \varepsilon X_x. \quad (4)$$

Here, $\alpha$ is the magnetic flux through the unit cell and $k_y$ is the wave vector in the perpendicular direction. For small magnetic fields $\alpha \ll 1$, the discreteness of the problem plays no role and the energy spectrum of Eq. (4) is a ladder of degenerate Landau levels for electrons moving along quantized cyclotron orbits. In the finite structure, the edge states of topological nature arise in the gaps between the Landau levels. Such states correspond to electrons moving along skipping orbits at the structure edge, and are the origin for the quantum Hall effect[22].

In our system, the ratio $j/N$ of the group number to the total number of atoms in Eq. (3) plays the same role as the magnetic field flux in Eq. (4). The spectrum also consists of degenerate Landau levels and the topological edge states in the gaps between them, see Fig. 3a. The result of exact numerical diagonalization of the two-polariton Hamiltonian Eq. (1) [bold symbols in Fig. 3a] agrees quantitatively with the solution of Eq. (3) [open symbols in Fig. 3a]. Thus, the states Eq. (2) exhibit nontrivial topology induced by interaction for each of the two indistinguishable polaritons.

The energy spectrum of the Harper Eq. (4) becomes very rich when the magnetic flux $\alpha$ increases. The Landau levels split and transform into a celebrated Hofstadter butterfly[38], shown also in Supplementary Fig. 2. The butterfly has a self-similar structure with $q$ allowed energy bands at the rational fluxes $\alpha = p/q$[37] and a Cantor-set spectrum for irrational fluxes. Even though in our case the effective magnetic flux $j/N$ is rational, we can still extract an analog of the Hofstadter butterfly from the two-polariton spectrum in Fig. 2e–g. We separate the groups of states in Fig. 2e–h formed by different standing waves (i.e., different effective magnetic fields) and align them horizontally, the details are presented in "Methods" and Supplementary Fig. 3. The resulting butterfly is shown in Fig. 3b and it qualitatively resembles the Hofstadter butterfly (Supplementary Fig. 2).

In accordance with Figs 2 and 3a, for small magnetic fluxes $j/N$ the butterfly in Fig. 3b features distinct Landau levels with edge states in the gaps between them. These edge states correspond to red points in Fig. 3b. At high magnetic fields the Landau levels split, but the spectrum still retains a surprisingly delicate structure.

## Polariton–polariton entanglement

The internal structure of the two-polariton states is represented by their entanglement entropy[60], $S = -\sum_{\nu=1}^{N} |\lambda_\nu| \ln |\lambda_\nu|$, obtained from the Schmidt expansion $\psi_{nm} = \sum_{\nu=1}^{N} \sqrt{\lambda_\nu}\psi_n^\nu \psi_m^\nu$, $(\Sigma\lambda_\nu = 1)$. The result, presented in Fig. 4b, demonstrates a rich variety of eigenstates with different localization degrees, indicated by the color. Characteristic examples of wavefunctions are shown in

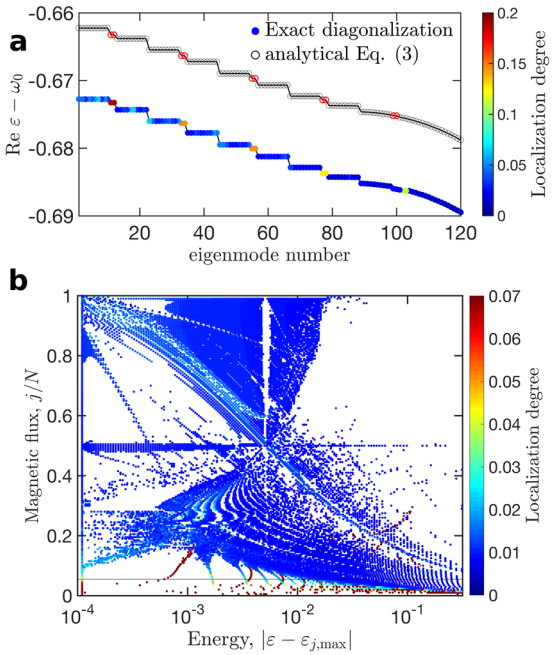


**Fig. 3 Self-induced Hofstadter butterfly. a** Energy spectrum for the two-polariton states in the group of states corresponding to $j = 11$, calculated from the approximate Eq. (3) and by the exact diagonalization of the two-particle Hamiltonian Eq. (1). **b** Butterfly energy spectrum obtained by the exact diagonalization as a function of group number $j$, determining the effective magnetic field. Localization degree is determined as the inverse participation ratio of the vector $\chi$ in Eq. (2) and is shown by color. Thin horizontal line in **b** indicates magnetic field $j/N = 11/200$, corresponding to panel **a**. Calculation has been performed for $N = 200$ and $\varphi = 0.02$, energy is measured in the units of $\Gamma_0$.

Fig. 4a. The entropy of entanglement gives an indication of the number of distinct constituent single-particle states in a two-body state, so it is low for the scattering states, where two polaritons are quasi-independent. The topological states Eq. (2) also have an intrinsically low entropy, being just a product of a standing wave and a localized or an edge state. However, the states Eq. (2) can mix with each other resulting in larger entanglement entropy. This entangled mixing becomes especially prominent for the Landau level states, cf. points LL, CIS, and ES in Fig. 4b. When the real part of energy approaches $\omega_0$ from the negative side, the mixing between different standing waves increases since the spectrum gets denser, and the states become chaotic-like, see also the top right corner of Fig. 1d. These chaotic-like states are characterized by an irregular wavefunction in the real space and a dense Fourier spectrum in the reciprocal space; they can not be reduced to a product of just two single-polariton states. The specific mechanism of chaotization requires a separate study. At very small negative energies $\varepsilon - \omega_0 \sim -\varphi\Gamma_0$ the single-particle dispersion changes from $\varepsilon \propto -1/k^2$ to $\varepsilon \propto -(k - \pi/d)^2$ because both polaritons get closer to the Brillouin zone edge, and the fermionic correlations[46] emerge from chaos. The dense group of two-polariton states in the right panel of Fig. 4b, where $\mathrm{Re}\,\varepsilon > 0$, is formed by the interaction with the quasi-superradiant mode with $\mathrm{Re}\,\varepsilon - \omega_0 \approx 71\Gamma_0$ in Fig. 2a. One of the states in this group has an entanglement entropy even higher than that of the chaotic-like states, as seen by the point labeled MES at $\mathrm{Re}\,\varepsilon - \omega_0 \approx 35\Gamma_0$. Similar to the chaotic-like state, the most entangled state can not be reduced to a product of just several single-polariton states, but its wavefunction looks more regular.

## DISCUSSION

We have discovered an interaction-induced internal topological order for the two-polariton states in a light-coupled one-dimensional atomic array.

Our results indicate that the platform of waveguide quantum electrodynamics has tremendous uncovered potential for quantum simulators of many-body interacting systems. The underlying Dicke-type model demonstrates an incredible diversity of quantum states with different topologies, lifetimes, and entanglement. Its unexplored richness may mean it will become as celebrated as well-known many-body physics models such as the Heisenberg model, Bose-Hubbard model, or the Luttinger liquid. The waveguide-mediated long-ranged couplings, intrinsic for the waveguide QED setup are quite uncharacteristic for traditional quantum systems and there is much more to explore. For example, we have focused here only on the regime of extremely subwavelength distances between the atoms, where two-polariton bound states[58,61] play no role. Polariton–polariton interactions could be even more interesting in Bragg-spaced lattices, where the non-Markovian effects are drastically enhanced[62–64]. The ultra-strong coupling regime[43] is also unexamined for these quantum waveguides to the best of our knowledge.

On the more practical side, the discovered topological two-polariton states could be used to engineer quantum optical correlations and protect them against the disorder and decoherence. First, since one of the two polaritons is in a deeply subradiant state, the radiative losses for the considered states can be practically neglected (see more detailed analysis in the Supplementary Information). It may also be possible to suppress the radiative losses more strongly by exploring the quantum regime of recently proposed high-quality states[65]. Second, our calculation (see Supplementary Figs 6 and 7) indicates that the interaction-induced edge states of the polaritons are protected from certain kinds of disorder. While the inhomogeneous broadening of the qubit energies relatively easily destroys topological states, they are quite robust against the fluctuations of the qubit positions. Even though the fine structure of the Landau level states is smeared out by the fluctuations, the edge states remain well localized. It is thus very interesting to study whether the proposed concept can be used to generate complex multi-photon states with built-in nontrivial topology. In the considered two-polariton case, one polariton is localized at the edge and another one is in the standing wave state or vice versa. One can also envisage topological N11N states, where one polariton in the standing wave state induces topological localization of $N > 1$ polaritons. Such quantum states could find applications in quantum metrology like high-N00N states[66].

## METHODS

### Analytical model for polariton–polariton interactions

In this section, we start from the Hamiltonian Eq. (1) in the main text[47,55] and proceed to derive Eq. (3) that describes the interaction between the two polaritons. Substituting the ansatz $|\Psi\rangle = \sum \psi_{mn}\sigma_n^\dagger\sigma_m^\dagger|0\rangle$ into the Schrödinger equation $H\Psi = 2\varepsilon\Psi$ we obtain the two-polariton Schrödinger equation in the form[47,48]

$$\mathcal{H}_{mn'}\psi_{n'n} + \psi_{mn'}\mathcal{H}_{n'n} - 2\delta_{mn}\mathcal{H}_{nn'}\psi_{n'n} = 2(\varepsilon - \omega_0)\psi_{mn}. \quad (5)$$

We note that Eq. (5) with the non-Hermitian Hamiltonian can be rigorously derived using conventional input-output approaches of quantum optics[67,68]. For example, another equivalent way to obtain the same results for double-excited states is to use the Linbdlad formalism for the density matrix of the system[68]. The double-excited eigenstates of the Hamiltonian Eq. (5) correspond to the resonances of the scattering matrix for two photons incident in the waveguide and interacting with the atomic array[47,67]. In order to obtain spatial resolution, the double-excited states could also be probed by addressing individual qubits[41] directly, rather than using the waveguide modes. In this case, it might be useful to explore the quantum tomography approach proposed in ref. [69].

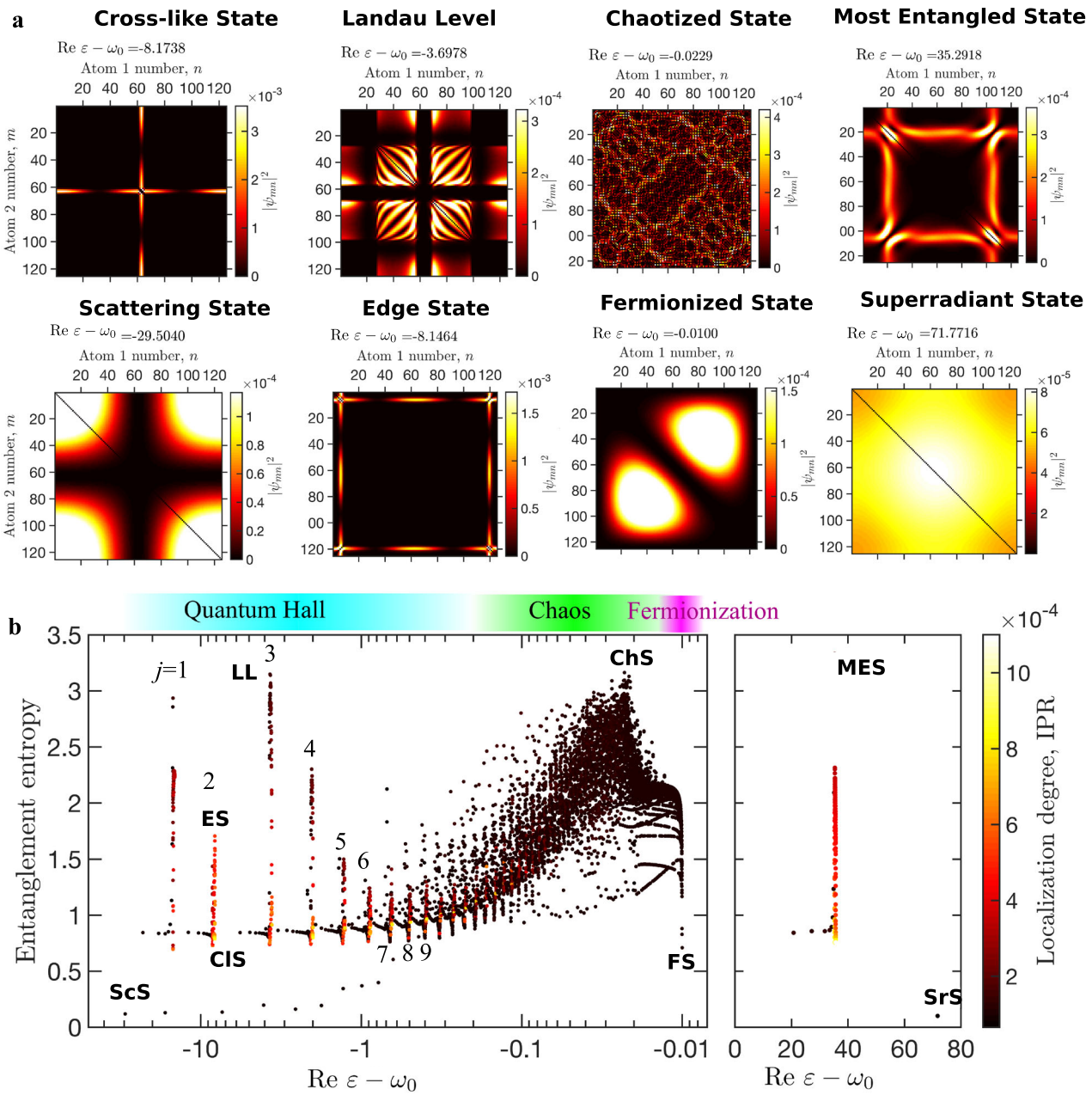


**Fig. 4 Diversity of two-polariton states. a** Characteristic wavefunctions for different types of two-polariton states, indicated in **b** by abbreviations. **b** Entanglement entropy depending on the state energy. Color shows the inverse participation ratio that characterizes the localization degree. Left and right panels correspond to the states with Re $\varepsilon < \omega_0$ and Re $\varepsilon > \omega_0$, respectively. Standing wave numbers $j$ are indicated near corresponding groups of states. Calculation has been performed for $N = 125$, $\omega_0 d/c = 0.02$. Energy is measured in the units of $\Gamma_0$.

This system is readily solved numerically after the wavefunction $\psi$ is rewritten in the basis of $N(N-1)/2$ localized states of the type

$$[\widetilde{\psi}]_{mn} = [\widetilde{\psi}]_{nm} = \frac{1}{\sqrt{2}}, \quad n \neq m.$$

Our next goal is to go beyond refs. [47,48,58] and obtain Eq. (3). To this end, we notice that[48,58]

$$K \equiv \mathcal{H}^{-1} \approx \tfrac{1}{2\varphi\Gamma_0}\partial^2, \text{ where } \partial^2 \equiv \begin{pmatrix} -1 & 1 & 0 & \dots \\ 1 & -2 & 1 & \dots \\ & & \ddots & \\ \dots & 1 & -2 & 1 \\ \dots & 0 & 1 & -1 \end{pmatrix}. \quad (6)$$

Here, the matrix $\partial^2$ represents the one-dimensional discrete Laplacian (or the operator of discrete second-order derivative). This means that for a vector $\psi_n$ with a smooth dependence on $n$, one has

$$[\partial^2\psi]_n = \psi_{n+1} + \psi_{n-1} - 2\psi_n \approx \frac{\mathrm{d}^2\psi_n}{\mathrm{d}n^2}.$$

Thus, for a short-period array with $\varphi \ll 1$ the operator $K$ reduces to the second derivative operator. The inverted Hamiltonian $K$ in Eq. (6) is a sparse matrix with only nearest-neighbor couplings. This fact inspires us to perform the transformation

$$\psi = K\psi' K \quad (7)$$

that means change of the basis to

$$|x\rangle = \frac{1}{\sqrt{N}}\sum_{n=1}^{N} e^{i\omega_0 d|x-n|/c}\sigma_n^\dagger|0\rangle, \text{ where } x = 1, 2, \ldots N. \quad (8)$$

This basis inherits the distribution of the electric field emitted by a given atom. Indeed, $\exp(i\omega_0 d|x-n|/c)$ is just the Green function for a photon in one dimension. Since the wave equations for the electric field are local, the transformed two-polariton Schrödinger equation will be local as well, i.e., it will involve only sparse matrices. Substituting Eq. (7) into Eq. (5) we find[48,58]

$$K_{xx'}\psi'_{x'y} + \psi'_{xy'}K_{y'y} - 2\delta_{xy}\psi_{xy'}K_{y'x} = 2(\varepsilon - \omega_0)K_{xx'}\psi'_{x'y'}K_{y'y}, \quad (9)$$

where summation over the dummy indices $x'$ and $y'$ is assumed. Next, we look for the solution to the transformed equation (9) in the form

$$\psi'_{xy} = \psi_y^{(j)}\chi_x + \psi_x^{(j)}\chi_y, \quad x, y = 1\ldots N, \quad (10)$$

corresponding to Eq. (2) in the main text. Here, one of the two excitations is a single-particle eigenstate of the matrix $\mathcal{H}$ with the eigenfrequency $\Omega_j$. The corresponding single-polariton eigenfrequency is $\omega_j = \omega_0 + \Omega_j$. Using the definition $K \equiv \mathcal{H}^{-1}$, we find

$$K\psi^{(j)} = \frac{1}{\Omega_j}\psi^{(j)}. \quad (11)$$

The state is normalized as $\sum_x [\psi_x^{(j)}]^2 = 1$. The normalization does not involve complex conjugation, because the original matrix $\mathcal{H}$ is not Hermitian but symmetric. As such, its eigenvectors $\psi^{(j)}$ satisfy the non-conjugated orthogonality condition $\langle j|j'\rangle \equiv \sum_{x=1}^{N}\psi_x^{(j)}\psi_x^{(j')} = \delta_{jj'}$. Owing to the translational symmetry the vector $\psi^{(j)}$ is just a standing wave[56]:

$$\psi_x^{(j)} \approx \sqrt{\frac{2}{N}}\cos\frac{\pi j(x-1/2)}{N}. \quad (12)$$

We note, that the ansatz (10) and (12), where the eigenstate $\psi^{(j)}$ does not take into account the interaction effects, works only for the transformed Schrödinger Eq. (9). This ansatz does not adequately describe the solutions to the original Eq. (5) because the wavefunction $\psi'$ does not turn to zero for $x = y$.

Substituting Eq. (10) into Eq. (9), multiplying the result by $\psi_y^{(j)}$ and summing over $y$ we obtain

$$\left[\frac{\chi_x}{\Omega_j} + K_{xy}\chi_y + \frac{2}{\Omega_j}\psi_x^{(j)}\psi_y^{(j)}\chi_y\right] - 2\psi_x^{(j),2}\left[\frac{1}{\Omega_j}\chi_x + K_{xy}\chi_y\right] = \frac{2(\varepsilon-\omega_0)}{\Omega_j}\left(K_{xy}\chi_y + \frac{1}{\Omega_j}\psi_x^{(j)}\psi_y^{(j)}\chi_y\right). \quad (13)$$

We are going to consider strongly localized eigenstates that are orthogonal to the standing wave $\psi^{(j)}$. Moreover, for relatively small $j$ the function $\chi$ changes with $x$ much faster than $\psi^{(j)}$. Hence, we neglect the terms $\propto \psi_x^{(j),2}\chi_x$ and $\propto \psi_x^{(j)}\psi_y^{(j)}\chi_y$ and find

$$\frac{\chi_x}{\Omega_j} + K_{xy}\chi_y - 2[(\psi^{(j),2})K]_{xy}\chi_y = \frac{2(\varepsilon-\omega_0)}{\Omega_j}K_{xy}\chi_y. \quad (14)$$

Taking Eq. (6) into account, we recover Eq. (3) from the main text.

## Fourier analysis of the eigenstates

The calculation of the energy spectrum of the Hamiltonian Eq. (1), shown in Fig. 2, is relatively straightforward. The spectrum is found by standard linear algebra techniques, and is described in more detail in the Supplementary Information. However, it is more challenging to extract the butterfly spectrum in Fig. 3b from the spectrum in Fig. 2e. This task requires careful separation of the groups of two-polariton states. We start by performing the Schmidt decomposition of the two-polariton state

$$\psi_{xy} = \sum_{\nu=1}^{N}\sqrt{\lambda_\nu}\psi_x^\nu\psi_y^\nu \quad (15)$$

for all the states that have $\mathrm{Re}\,\varepsilon < \omega_0$ with unconjugated orthogonality condition $\sum_x \psi_x^\nu\psi_x^\mu = \delta_{\mu\nu}$. The form of decomposition Eq. (15) where left and right singular vectors are the same enforces the symmetricity condition $\psi_{xy} = \psi_{yx}$. Our analysis of the Schmidt decomposition confirms that most states are well approximated using the two largest singular values $\lambda_1$ and $\lambda_2$, that have close absolute values. Keeping only these two terms, we obtain linear combinations of the wavefunctions $\psi_x^1$ and $\psi_y^2$ as $u_n^\pm = \lambda_1^{-1/4}\psi_n^1 \pm i\lambda_2^{-1/4}\psi_n^2$. After that, the two-polariton state can be approximately presented as $\psi_{xy} \propto u_x^+u_y^- + u_x^-u_y^+$. Next, we select one of the two states $u_x^+$, $u_y^-$ that has lower inverse participation ratio, $\sum|u_x|^4/[\sum|u_x|^2]^2$, which means it is less localized in space. We designate this state as $u^{(\mathrm{free})}$ and the more localized one as $u^{(\mathrm{loc})}$, perform the discrete Fourier transform

$$u^{(\mathrm{free})}(k) = \sum_{x=1}^{N} e^{-ikx}u_x^{(\mathrm{free})} \quad (16)$$

and calculate the wave vector $k_{\max}$, corresponding to the maximum of the Fourier decomposition. The number of the group can be then determined from the quantization rule

$$j \approx \left[\frac{k_{\max}N}{\pi}\right], \quad (17)$$

where square brackets indicate the rounding to the nearest integer. In order to improve the precision in Eq. (17) for large $j$, we also characterize the vectors $\chi$ by their mirror symmetry. Then we apply Eq. (17) separately for odd and even states with odd and even $j$, respectively. The results of Fourier transform for $N = 200$ atoms are shown in Supplementary Figs 3 and 4. Except for very large $j$ close to $N$, the spectrum is clearly separated into well-defined steps of alternating parity. There is an exception of several outlier states with $26 \le k_{\max}N/\pi \lesssim 41$ and smaller values of $|\mathrm{Re}\,\varepsilon - \omega_0 < 10^{-1}|$ that can be seen in lower left corner of Fig. S3. We exclude these states from our analysis and do not put them on the butterfly spectrum Fig. 3b. Another type of outlier states have $k_{\max}N/\pi \sim 50$ and different distinct values of energies in the range $10^0\Gamma_0 \le -\mathrm{Re}\,\varepsilon + \omega_0 \le 10^1\Gamma_0$ (lower right quarter of Fig. S3). They are out of the scope of the current manuscript but do not require any special exclusion procedure. Next, we assign each step to a different group of eigenvalues and align the groups with respect to each other. This is done by subtracting the energy with the largest (smallest negative) real part from the energies of the states of each group, $\varepsilon_{j,max}$. In order to keep the points with the highest energy on the semilogarithmic plot after this subtraction, we also add a small value of $1.1\times10^{-4}\Gamma_0$ to all the energies. The result is the butterfly spectrum, shown in Fig. 3b.

## DATA AVAILABILITY

The data files used to prepare the figures shown in the manuscript are available from the last corresponding author upon request.

Received: 14 July 2020; Accepted: 6 January 2021;
Published online: 16 February 2021

## REFERENCES

1. Gu, X., Kockum, A. F., Miranowicz, A., xi Liu, Y. & Nori, F. Microwave photonics with superconducting quantum circuits. *Phys. Rep.* **718-719**, 1 – 102 (2017).
2. Clerk, A. A., Lehnert, K. W., Bertet, P., Petta, J. R. & Nakamura, Y. Hybrid quantum systems with circuit quantum electrodynamics. *Nat. Phys.* **16**, 257–267 (2020).
3. Haroche, S., Brune, M. & Raimond, J. M. From cavity to circuit quantum electrodynamics. *Nat. Phys.* **16**, 243–246 (2020).
4. Roy, D., Wilson, C. M. & Firstenberg, O. *Colloquium:* strongly interacting photons in one-dimensional continuum. *Rev. Mod. Phys.* **89**, 021001 (2017).
5. Chang, D. E., Douglas, J. S., González-Tudela, A., Hung, C.-L. & Kimble, H. J. *Colloquium:* quantum matter built from nanoscopic lattices of atoms and photons. *Rev. Mod. Phys.* **90**, 031002 (2018).
6. Corzo, N. V. et al. Waveguide-coupled single collective excitation of atomic arrays. *Nature* **566**, 359–362 (2019).
7. Sipahigil, A. et al. An integrated diamond nanophotonics platform for quantum-optical networks. *Science* **354**, 847–850 (2016).
8. Astafiev, O. et al. Resonance fluorescence of a single artificial atom. *Science* **327**, 840–843 (2010).
9. Wang, Z. et al. Controllable switching between superradiant and subradiant states in a 10-qubit superconducting circuit. *Phys. Rev. Lett.* **124**, 013601 (2020).
10. Browaeys, A. & Lahaye, T. Many-body physics with individually controlled Rydberg atoms. *Nat. Phys.* **16**, 132–142 (2020).
11. Blais, A., Girvin, S. M. & Oliver, W. D. Quantum information processing and quantum optics with circuit quantum electrodynamics. *Nat. Phys.* **16**, 247–256 (2020).
12. Carusotto, I. et al. Photonic materials in circuit quantum electrodynamics. *Nat. Phys.* **16**, 268–279 (2020).
13. Ghosh, S. & Liew, T. C. H. Quantum computing with exciton-polariton condensates. *NPJ Quant. Inf* **6**, 16 (2020).

14. González-Tudela, A., Paulisch, V., Kimble, H. J. & Cirac, J. I. Efficient multiphoton generation in waveguide quantum electrodynamics. *Phys. Rev. Lett.* **118**, 213601 (2017).
15. Paulisch, V., Kimble, H. J., Cirac, J. I. & González-Tudela, A. Generation of single- and two-mode multiphoton states in waveguide QED. *Phys. Rev. A* **97**, 053831 (2018).
16. Zhang, X. H. & Baranger, H. U. Heralded Bell state of dissipative qubits using classical light in a waveguide. *Phys. Rev. Lett.* **122**, 140502 (2019).
17. Malz, D. & Cirac, J. I. Nondestructive photon counting in waveguide QED. *Phys. Rev. Res.* **2**, 033091 (2020).
18. Everett, J. L., Higginbottom, D. B., Campbell, G. T., Lam, P. K. & Buchler, B. C. Stationary light in atomic media. *Adv. Quant. Technol.* **2**, 1800100 (2019).
19. Leung, P. M. & Sanders, B. C. Coherent control of microwave pulse storage in superconducting circuits. *Phys. Rev. Lett.* **109**, 253603 (2012).
20. Buluta, I. & Nori, F. Quantum simulators. *Science* **326**, 108–111 (2009).
21. Georgescu, I. M., Ashhab, S. & Nori, F. Quantum simulation. *Rev. Mod. Phys.* **86**, 153–185 (2014).
22. Thouless, D. J., Kohmoto, M., Nightingale, M. P. & den Nijs, M. Quantized Hall conductance in a two-dimensional periodic potential. *Phys. Rev. Lett.* **49**, 405–408 (1982).
23. Gerchikov, L. G. & Subashiev, A. V. Interface states in subband structure of semiconductor quantum wells. *Phys. Status Solidi B* **160**, 443–457 (1990).
24. Bernevig, B. A., Hughes, T. L. & Zhang, S.-C. Quantum spin Hall effect and topological phase transition in HgTe quantum wells. *Science* **314**, 1757–1761 (2006).
25. Hasan, M. Z. & Kane, C. L. *Colloquium* : topological insulators. *Rev. Mod. Phys.* **82**, 3045–3067 (2010).
26. Ozawa, T. et al. Topological photonics. *Rev. Mod. Phys.* **91**, 015006 (2019).
27. Wang, Z., Chong, Y., Joannopoulos, J. D. & Soljačić, M. Observation of unidirectional backscattering-immune topological electromagnetic states. *Nature* **461**, 772–775 (2009).
28. Haldane, F. D. M. & Raghu, S. Possible realization of directional optical waveguides in photonic crystals with broken time-reversal symmetry. *Phys. Rev. Lett.* **100**, 013904 (2008).
29. Perczel, J., Borregaard, J., Chang, D. E., Yelin, S. F. & Lukin, M. D. Topological quantum optics using atomlike emitter arrays coupled to photonic crystals. *Phys. Rev. Lett.* **124**, 083603 (2020).
30. Khanikaev, A. B. & Shvets, G. Two-dimensional topological photonics. *Nat. Photon.* **11**, 763–773 (2017).
31. Hauke, P. et al. Non-abelian gauge fields and topological insulators in shaken optical lattices. *Phys. Rev. Lett.* **109**, 145301 (2012).
32. Sounas, D. L. & Alù, A. Non-reciprocal photonics based on time modulation. *Nat. Photon.* **11**, 774–783 (2017).
33. Roushan, P. et al. Spectroscopic signatures of localization with interacting photons in superconducting qubits. *Science* **358**, 1175–1179 (2017).
34. Dutt, A. et al. A single photonic cavity with two independent physical synthetic dimensions. *Science* **367**, 59–64 (2019).
35. Hadad, Y., Soric, J. C., Khanikaev, A. B. & Alù, A. Self-induced topological protection in nonlinear circuit arrays. *Nat. Electron.* **1**, 178–182 (2018).
36. Smirnova, D., Leykam, D., Chong, Y. & Kivshar, Y. Nonlinear topological photonics. *Appl. Phys. Rev.* **7**, 021306 (2020).
37. Azbel, M. Y. Energy spectrum of a conduction electron in a magnetic field. *Sov. Phys. JETP* **19**, 634 (1964).
38. Hofstadter, D. R. Energy levels and wave functions of Bloch electrons in rational and irrational magnetic fields. *Phys. Rev. B* **14**, 2239–2249 (1976).
39. Dean, C. R. et al. Hofstadter's butterfly and the fractal quantum Hall effect in moiré superlattices. *Nature* **497**, 598–602 (2013).
40. Mirhosseini, M. et al. Cavity quantum electrodynamics with atom-like mirrors. *Nature* **569**, 692–697 (2019).
41. Yan, Z. et al. Strongly correlated quantum walks with a 12-qubit superconducting processor. *Science* **364**, 753–756 (2019).
42. Birnbaum, K. M. et al. Photon blockade in an optical cavity with one trapped atom. *Nature* **436**, 87–90 (2005).
43. Kockum, A. F., Miranowicz, A., Liberato, S. D., Savasta, S. & Nori, F. Ultrastrong coupling between light and matter. *Nat. Rev. Phys.* **1**, 19–40 (2019).
44. Dicke, R. H. Coherence in spontaneous radiation processes. *Phys. Rev.* **93**, 99 (1954).
45. Shammah, N., Lambert, N., Nori, F. & De Liberato, S. Superradiance with local phase-breaking effects. *Phys. Rev. A* **96**, 023863 (2017).
46. Zhang, Y.-X. & Mølmer, K. Theory of subradiant states of a one-dimensional two-level atom chain. *Phys. Rev. Lett.* **122**, 203605 (2019).
47. Ke, Y., Poshakinskiy, A. V., Lee, C., Kivshar, Y. S. & Poddubny, A. N. Inelastic scattering of photon pairs in qubit arrays with subradiant states. *Phys. Rev. Lett.* **123**, 253601 (2019).
48. Zhong, J. et al. Photon-mediated localization in two-level qubit arrays. *Phys. Rev. Lett.* **124**, 093604 (2020).
49. Aubry, S. & André, G. Analyticity breaking and Anderson localization in incommensurate lattices. *Ann. Isr. Phys. Soc.* **3**, 133 (1980).
50. Kraus, Y. E., Lahini, Y., Ringel, Z., Verbin, M. & Zilberberg, O. Topological states and adiabatic pumping in quasicrystals. *Phys. Rev. Lett.* **109**, 106402 (2012).
51. Poshakinskiy, A., Poddubny, A., Pilozzi, L. & Ivchenko, E. Radiative topological states in resonant photonic crystals. *Phys. Rev. Lett.* **112**, 107403 (2014).
52. Baboux, F. et al. Measuring topological invariants from generalized edge states in polaritonic quasicrystals. *Phys. Rev. B* **95**, 161114 (2017).
53. Ke, Y. et al. Radiative topological biphoton states in modulated qubit arrays. *Phys. Rev. Res.* **2**, 033190 (2020).
54. Verbin, M., Zilberberg, O., Kraus, Y. E., Lahini, Y. & Silberberg, Y. Observation of topological phase transitions in photonic quasicrystals. *Phys. Rev. Lett.* **110**, 076403 (2013).
55. Albrecht, A. et al. Subradiant states of quantum bits coupled to a one-dimensional waveguide. *N. J. Phys.* **21**, 025003 (2019).
56. Ivchenko, E. L. Excitonic polaritons in periodic quantum-well structures. *Sov. Phys. Sol. State* **33**, 1344–1346 (1991).
57. Vladimirova, M. R., Ivchenko, E. L. & Kavokin, A. V. Exciton polaritons in long-period quantum-well structures. *Semiconductors* **32**, 90–95 (1998).
58. Poddubny, A. N. Quasiflat band enabling subradiant two-photon bound states. *Phys. Rev. A* **101**, 043845 (2020).
59. Harper, P. G. Single band motion of conduction electrons in a uniform magnetic field. *Proc. Phys. Soc. Lond. A* **68**, 874 (1955).
60. Eisert, J., Cramer, M. & Plenio, M. B. *Colloquium:* area laws for the entanglement entropy. *Rev. Mod. Phys.* **82**, 277–306 (2010).
61. Zhang, Y.-X., Yu, C. & Mølmer, K. Subradiant bound dimer excited states of emitter chains coupled to a one dimensional waveguide. *Phys. Rev. Res.* **2**, 013173 (2020).
62. Ivchenko, E. L., Nesvizhskii, A. I. & Jorda, S. Bragg reflection of light from quantum-well structures. *Phys. Solid State* **36**, 1156–1161 (1994).
63. Hübner, M. et al. Optical lattices achieved by excitons in periodic quantum well structures. *Phys. Rev. Lett.* **83**, 2841–2844 (1999).
64. Goldberg, D. et al. Exciton-lattice polaritons in multiple-quantum-well-based photonic crystals. *Nat. Photon.* **3**, 662–666 (2009).
65. Koshelev, K. et al. Subwavelength dielectric resonators for nonlinear nanophotonics. *Science* **367**, 288–292 (2020).
66. Afek, I., Ambar, O. & Silberberg, Y. High-NOON states by mixing quantum and classical light. *Science* **328**, 879–881 (2010).
67. Fang, Y.-L. L., Zheng, H. & Baranger, H. U. One-dimensional waveguide coupled to multiple qubits: photon-photon correlations. *EPJ Quant. Technol.* **1**, 3 (2014).
68. Lalumière, K. et al. Input-output theory for waveguide QED with an ensemble of inhomogeneous atoms. *Phys. Rev. A* **88**, 043806 (2013).
69. Gorlach, M. A. et al. Simulation of two-boson bound states using arrays of driven-dissipative coupled linear optical resonators. *Phys. Rev. A* **98**, 063625 (2018).

## ACKNOWLEDGEMENTS

This work was supported by the Australian Research Council. J.Z. was supported by Australian Government Research Training Program (RTP) Scholarship. C.L. was supported by the National Natural Science Foundation of China (NNSFC) (grants No. 11874434 and No. 11574405). Y.K. was partially supported by the Office of China Postdoctoral Council (grant No. 20180052), the National Natural Science Foundation of China (grant No. 11904419), and the Australian Research Council (DP200101168). A.V.P. acknowledges a support from the Russian Science Foundation (Project No. 19-72-00080). A.N.P. and N.A. O. acknowledge partial support by the Russian President Grant No. MD-243.2020.2. N.A. O. has been partially supported by the Foundation for the Advancement of Theoretical Physics and Mathematics "BASIS."

## AUTHOR CONTRIBUTIONS

A.N.P. and A.V.P. conceived the idea and developed an analytical model. J.Z., A.N.P., N.A. O., and Y.K. performed the numerical calculations. A.N.P., C.L., and Y.S.K. supervised the project. All authors contributed to discussion of the results and writing the manuscript.

## COMPETING INTERESTS

The authors declare no competing interests.

## ADDITIONAL INFORMATION

**Supplementary information** The online version contains supplementary material available at https://doi.org/10.1038/s41534-021-00372-8.

**Correspondence** and requests for materials should be addressed to Y.S.K. or A.N.P.

**Reprints and permission information** is available at http://www.nature.com/reprints